arXiv:1406.3804v2 [cond-mat.supr-con] 6 Oct 2014

Crossed surface flat bands of Weyl semimetal superconductors

Bo Lu, Keiji Yada, Masatoshi Sato, and Yukio Tanaka
Department of Applied Physics, Nagoya University, Nagoya 464-8603, Japan
(Dated: February 29, 2024)

It has been noted that certain surfaces of Weyl semimetals have bound states forming open Fermi arcs, which are never seen in typical metallic states. We show that the Fermi arcs enable them to support an even more exotic surface state with *crossed* flat bands in the superconducting state. We clarify the topological origin of the crossed flat bands and the relevant symmetry that stabilizes the cross point. We also discuss their possible experimental verification by tunneling spectroscopy.

PACS numbers: 74.50.+r, 73.20.-r, 74.20.Rp, 03.65.Vf

Introduction.– Weyl semimetals (WSMs) are three-dimensional materials that support pairs of bulk gapless points that are effectively described by Weyl fermions [1–9]. The characteristic band-touching points may be viewed as topological magnetic monopoles in momentum space, which predicts many interesting phenomena such as anomalous Hall effects, chiral anomalies [10–15], and magneto-electric effects [16–20]. Candidate materials include pyrochlore iridates [2], $HgCr_2Se_4$ [3, 21] and magnetically doped Bi_2Se_3 family [7, 22]. A simpler realization in a topological insulator multilayer has also been proposed [4, 23]. The most fundamental and striking prediction for WSMs is the existence of Fermi *arcs* on their boundary [2, 24]. Whereas ordinary electrons in metals form closed Fermi surfaces in momentum space, the surface bound states of WSMs form open arcs at the Fermi energy, not closed circles. The Fermi arcs reported in experimental studies of high-T_c cuprate superconductors were not true arcs, but the suppression of the density of states due to the formation of pseudogap states [25]. In contrast, WSMs host true arcs that are terminated by the projection of band-touching Weyl points on the surface Brillouin zone (BZ). Such exotic states may carry topological flows, so they provide the aforementioned variety of nontrivial phenomena in low-energy physics. WSMs require breaking time-reversal or inversion symmetry [4]. Below we consider time-reversal breaking WSMs.

Upon slight doping, WSMs have disconnected Fermi surfaces, each of which surrounds one of the band-touching Weyl points. It has been studied that either spacial uniform (e.g., BCS s-wave) or nonuniform (e.g., Fulde–Ferrell–Larkin–Ovchinnikov (FFLO) state) Cooper pairing can be formed on these Fermi surfaces [26–29]. Interestingly, the uniform superconducting state is found to support bulk gap nodes on the Fermi surface even for a constant s-wave pairing [26].

In this letter, we show that the nodal superconducting WSMs may support even more exotic surface bound states than Fermi arcs: The novel surface states form *crossed* flat bands, not simple arcs. Like Weyl points, nodes (antinodes) in superconducting states generally have positive (negative) monopole charges in momentum space. Thus, there are topological flows from nodes (or to antinodes), and corresponding surface zero energy flat bands are produced. We find that in the nodal superconducting state in WSMs, each Fermi surface supports only nodes (or only antinodes). Consequently, there arises a topological twist in the dispersion of the surface Andreev bound states (SABSs), which make it possible to realize such a complicated surface band structure.

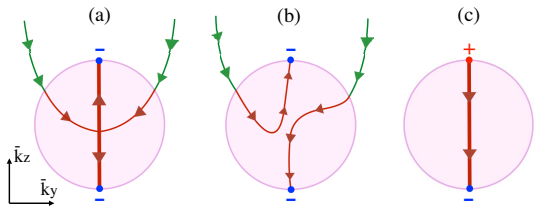


FIG. 1. (color online). Schematic illustration of surface flat bands in doped superconducting WSMs (a) with and (b) without magnetic mirror reflection symmetry, and (c) that for ^{3}He-A phase. The shaded circle (dots) indicates the Fermi surface (point nodes) projected on the surface BZ. The inserted signs at point nodes correspond to the signs of monopole charge. Arrows show the topological flows and are regarded as the zero energy flat bands. Simultaneously, the directions of the arrows show the chirality of the surface states: The zero energy flat band has a rightward group velocity when facing the direction of the arrows.

Figure 1(a) illustrates how such a topological twist occurs. A key ingredient is surface Fermi arcs in WSMs: The Fermi arcs in time-reversal breaking WSMs does not have a Kramers partner, which is necessary to form its BCS Cooper pair. Thus, the Fermi arcs remain as surface gapless modes even in the superconducting state. In the Nambu representation, we also have surface Fermi arcs of holes as well as those of electrons. Near the projected Fermi surface on the surface BZ, they merge into the zero energy SABS, as illustrated in Fig.1(a). Preserving the topological flow denoted by arrows, these zero energy flat bands bend at a crossing point and they are terminated at the projection of antinodes. Note that a similar merging of surface states has been reported for superconducting topological insulators [30–32], although the relevant topological number and obtained spectrum

are completely different. Later, on the basis of symmetry and topology, we will argue that the existence of the crossing point of the flat bands is rather general. Such crossed band structures strongly enhance the surface density of states, which might induce nontrivial low-energy phenomena. Our findings also extend the possibility of controlling zero energy flat bands [33].

In the following, using a concrete model of WSMs, we demonstrate crossed surface flat bands in an s-wave superconducting state. Then, we identify the topological number responsible for the exotic band structure and embody the topological arguments given above. We will also discuss the experimental signatures. We use $\hbar = 1$ units and take the lattice spacing a as $a = 1$.

Model.–As a model of WSMs with an s-wave pairing, we use the two-band Hamiltonian $H = \frac{1}{2}\sum_{\boldsymbol{k}} \hat{c}^\dagger_{\boldsymbol{k}} \mathcal{H}_{\boldsymbol{k}} \hat{c}_{\boldsymbol{k}}$ [26, 34] with

$$\mathcal{H}_{\boldsymbol{k}} = t\sin k_x \sigma_y\tau_z - t\sin k_y\sigma_x\tau_0 + (t_z\cos k_z - M)\sigma_z\tau_z \\ +m(2-\cos k_x - \cos k_y)\sigma_z\tau_z - \mu\sigma_0\tau_z - \Delta\sigma_y\tau_y, \qquad (1)$$

where the spinor $\hat{c}_k$ is given by $(c_{k\uparrow}, c_{k\downarrow}, c^\dagger_{-k\uparrow}, c^\dagger_{-k\downarrow})^T$, σ_i (τ_i) is the Pauli matrix in spin (Nambu) space, and t (t_z) is the hopping in the k_x–k_y plane (along the k_z-axis). $M(\equiv t_z\cos Q)$ denotes a magnetic order or a Zeeman field that breaks the time-reversal symmetry, μ is the chemical potential, and Δ is a conventional s-wave pair potential. We also introduce a parameter m to control the position of the Weyl points. When $m = 0$, the normal state ($\Delta = 0$) possesses four pairs of bands touching Weyl points at $(0, 0, \pm Q)$, $(\pi, 0, \pm Q)$, $(0, \pi, \pm Q)$, and $(\pi, \pi, \pm Q)$, respectively. Hence, upon slight doping with small μ, we have eight disconnected Fermi surfaces, each of which surrounds a Weyl point. When m is turned on, however, the latter three pairs of Weyl points located on the BZ boundary move; for large m, they pair-annihilate. Correspondingly, only two disconnected Fermi surfaces surrounding Weyl points at $(0, 0, \pm Q)$ survive.

Each Fermi surface of the doped WSM, in contrast to those of ordinary metals, does not have spin degeneracy because of time-reversal breaking and strong spin–orbit interaction. The spin and momentum are locked on the Fermi surface, so a spinless system is realized effectively. In this situation, even an s-wave pairing may host topological superconductivity [35–41]. In the present case, the simplest choice of the pair potential generates point nodes of the superconducting gap at the north and south poles of the Fermi surfaces [26].

Surface Andreev bound states.– Surface Andreev bound states (SABSs) [42–45] are a powerful probe of topological superconductivity because they directly reflect bulk topological structures [46–48]. To identify the nodal topological superconductivity in doped WSMs, we now examine the SABSs. Using an efficient way to calculate the lattice Green's function [49], we can obtain the SABSs from the poles of the Green's function. We choose the surface perpendicular to the x direction.

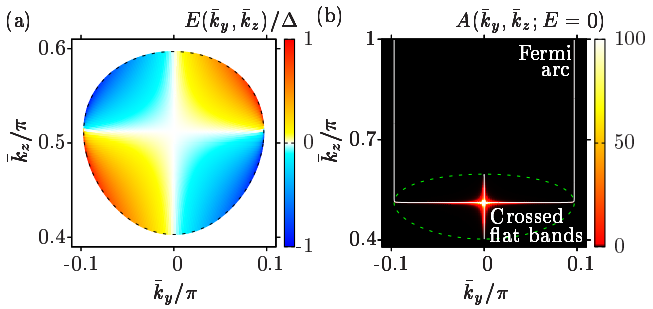


FIG. 2. (color online) (a) Energy dispersion $E\left(\bar{k}_y, \bar{k}_z\right)$ of SABS inside the projected Fermi surface near $(0, 0, Q)$. (b) Quasiparticle spectra function at zero energy. Dashed line denotes the projected Fermi surface. $t = t_z = 1$, $Q = \pi/2$, $\mu = 0.3$, $\Delta = 0.001$, and $m = 0.8$ are chosen for both (a) and (b).

Figure 2(a) shows the obtained SABSs. The model parameters are chosen so that the WSM has only two disconnected Fermi surfaces in the normal state. We show only the SABS in the upper half-plane ($\bar{k}_z > 0$) of the surface BZ, but a similar SABS exists in the lower half-plane ($\bar{k}_z < 0$). Clearly, Fig.2(a) indicates that the SABS hosts a twisted energy dispersion with two crossed flat bands extended in the vertical and horizontal directions, respectively. To be specific, consider the spectrum in the $\bar{k}_y$ direction. For a fixed $\bar{k}_z$, the SABS appears as a chiral edge mode with a linear dispersion, $E = v(\bar{k}_z)\bar{k}_y$, for small $\bar{k}_y$. The group velocity $v(\bar{k}_z)$ becomes zero at the position of the horizontal flat band, and the sign of $v(\bar{k}_z)$ is reversed when the chiral mode crosses the horizontal flat band. We also find that the horizontal flat band eventually becomes Fermi arcs, as illustrated in Fig.2(b).

The crossed flat band structure can also be confirmed by quasiclassical analysis. Consider a semi-infinite superconducting WSM placed on the right ($x > 0$) with a semi-infinite insulator on the left ($x < 0$). This can be done by replacing the parameters Δ and M in Eq. (1) with $\Delta\Theta(x)$ and $t_z\cos Q + M_0\Theta(-x)$, respectively. A large M_0 is chosen so that the left side does not have Weyl cones and thus become insulating. For weak pairing $0 < \Delta \ll \mu$, we can use the quasiclassical BdG Hamiltonian,

$$\mathcal{H}{=}it_z\sin Q\partial_z\sigma_z\tau_z - it(\partial_x\sigma_y\tau_z - \partial_y\sigma_x\tau_0) - \mu\sigma_0\tau_z \\ -\Delta\Theta(x)\sigma_y\tau_y - M_0\Theta(-x)\sigma_z\tau_z, \qquad (2)$$

near the Weyl point at $(0, 0, Q)$. The solution of the BdG equation $\mathcal{H}\Psi(r) = E\Psi(r)$ is given by $\Psi(r) = e^{i\bar{k}_y y + i(\bar{k}_z - Q)z}[\Psi_{\rm I}(x)\Theta(-x) + \Psi_{\rm S}(x)\Theta(x)]$ with

$$\Psi_{\rm I}(x) = [s_e\Psi_{e1} + s_h\Psi_{h1}]e^{\kappa x}, \\ \Psi_{\rm S}(x) = t_e\Psi_{et}e^{ik^e_x x} + t_h\Psi_{ht}e^{-ik^h_x x}. \qquad (3)$$

Here $k_x^{e(h)} = \sqrt{q_1^2 - \bar{k}_y^2 - (q_1/q_2)^2\left(\bar{k}_z - Q\right)^2} \pm i\zeta$ and $\kappa t = \sqrt{[(t_z \sin Q)(\bar{k}_z - Q) + M_0]^2 + t^2\bar{k}_y^2 - \mu^2}$, with $q_1 = \mu/t$, $q_2 = \mu/(t_z \sin Q)$ and $\zeta = \frac{\sqrt{\Delta^2 \sin^2\beta - E^2}}{t \sin\beta \cos\phi}$. With the parametrization of $\bar{k}_y = q_1 \sin\beta \sin\phi$ and $\bar{k}_z = q_2 \cos\beta + Q$, the four component amplitudes are given by $\Psi_{e1} = [t(\kappa + \bar{k}_y), -\eta, 0, 0]^T$, $\Psi_{h1} = [0, 0, t(-\kappa + \bar{k}_y), \eta]^T$, $\Psi_{et} = [\gamma \tan(\beta/2), i\gamma e^{i\phi}, -ie^{i\phi}\tan(\beta/2), 1]^T$, and $\Psi_{ht} = [\tan(\beta/2), -ie^{-i\phi}, i\gamma e^{-i\phi}\tan(\beta/2), \gamma]^T$, where $\eta = M_0 + \mu + (t_z \sin Q)(\bar{k}_z - Q)$, and $\gamma = \frac{\sqrt{E + \sqrt{E^2 - \Delta^2 \sin^2\beta}}}{\sqrt{E - \sqrt{E^2 - \Delta^2 \sin^2\beta}}}$. The coefficients $(s_{e(h)}, t_{e(h)})$ and the energy E are determined so as to satisfy the boundary condition $\Psi_I(0) = \Psi_S(0)$. Then, we obtain the energy dispersion as

$$E = \Delta \bar{k}_y (\bar{k}_z - Q)/(q_2 \sqrt{q_1^2 - \bar{k}_y^2}), \tag{4}$$

which clearly shows two flat bands along $\bar{k}_y = 0$ and $\bar{k}_z = Q$, respectively. We also find that the group velocity $v(\bar{k}_z) = \partial E/\partial \bar{k}_y$ reverses its sign at $\bar{k}_z = Q$, as expected.

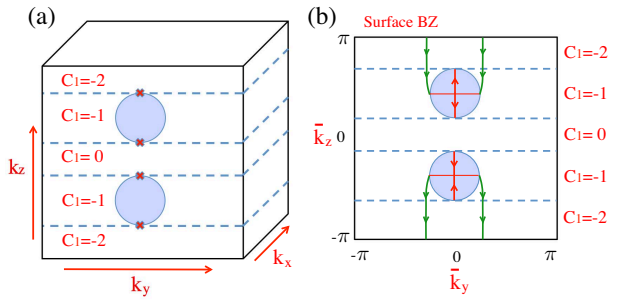


FIG. 3. (color online) (a) Projection of Fermi surfaces (dark region) on $\bar{k}_y - \bar{k}_z$ surface BZ and Chern number at a given k_z in the BZ. The Chern number $C_1(k_z)$ changes when k_z crosses a plane including a point node (red cross). The amount of change is given by the monopole charge of the point node. (b) Flat bands of SABS and Fermi arcs (lines with arrows) in the surface BZ.

Topological Analysis.– Now we would like to identify the bulk topology relevant to the crossed surface flat bands, which reveals that the unusual band structure is rather general for nodal superconducting states of WSMs. For simplicity, we consider the simplest case with two disconnected Fermi surfaces separated in the k_z direction, but more complicated cases can be discussed similarly.

As mentioned above, point nodes in superconducting WSMs behave like monopoles in momentum space. Each point node is a source or sink of the flux of the U(1) gauge field, $\mathcal{A}(\boldsymbol{k}) = i\sum_{E_n<0}\langle u_n(\boldsymbol{k})|\nabla_{\boldsymbol{k}}|u_n(\boldsymbol{k})\rangle$, where $|u_n(\boldsymbol{k})\rangle$ is a bulk occupied state of the BdG Hamiltonian, and the summation is taken for all occupied states. To capture the topological structure, consider a plane S that is normal to the k_z-axis in the BZ. If S does not contain any point nodes, the total flux (over 2π) penetrating S defines the first Chern number, $C_1(k_z) = \frac{1}{2\pi}\int_S d^2k\,[\nabla_{\boldsymbol{k}} \times \mathcal{A}(\boldsymbol{k})]_z$, where k_z is the position of S. The Chern number is a topological invariant that remains the same unless S touches a gap-closing point. When S crosses a point node, however, the Chern number changes. The change is equal to the total flux leaving the point node; thus, it provides its monopole charge.

When S is not close to the Fermi surface, the Chern number can be evaluated rather easily. In this case, we can turn off Δ without gap closing. Therefore, the Chern number is essentially the same as that in the normal state, though we have to take into account the contribution from holes as well as electrons. For inversion-symmetric WSMs, the hole and electron contributions are found to be the same, so the Chern number is doubled. For instance, if the Chern number of electrons is -1 (0) when the projection of S on the surface BZ crosses (does not cross) a Fermi arc, in the superconducting state it becomes -2 (remains 0) if S does not overlap the Fermi surface.

This simple calculation gives an alternative explanation of why the Fermi arcs remain in the superconducting state. From the surface–boundary correspondence, a nonzero bulk Chern number in WSMs ensures the existence of a Fermi arc; thus, if the Chern number is doubled, the number of Fermi arcs is also doubled by adding those of holes. The resulting Fermi arcs remain gapless even in the superconducting state.

Interestingly, the same calculation also explains why point nodes arise in the superconducting state. Because each Fermi surface surrounds a Weyl point, at least two Fermi arcs (i.e., those of holes and electrons) enter the projection of the Fermi surface on the surface BZ. From the above calculation, the Chern number corresponding to the remaining Fermi arcs should be even and nonzero, so a net flux of the U(1) gauge field $\mathcal{A}(\boldsymbol{k})$ also enters the Fermi surface. Therefore, flux conservation implies that there must be a source or sink of flux near the Fermi surface. In the normal state, the Weyl point is exactly the required source or sink, but in the superconducting state, it cannot be because it is below (or above) the Fermi level in the doped WSMs, so the Weyl point can no longer provide a monopole charge. Alternatively, we must have an even number of superconducting gap nodes on the Fermi surface, which supply a nonzero total monopole charge. Figure 3 shows the Chern numbers and corresponding SABSs in our model; the expected topological structures are indeed realized.

Now we would like to explain the topological stability of the crossed structure of the surface flat band: Although time-reversal symmetry is broken in WSMs, a combination of time-reversal and mirror reflection, which we call as magnetic mirror reflection, can be preserved. Actually, as well as the present model, candidate materials of WSMs such as pyrochlore iridates, $HgCr_2Se_4$,

and a topological insulator multilayer retain such magnetic mirror reflection symmetry. Then if the surface of a WSM also keeps magnetic mirror reflection symmetry, the surface flat bands should be symmetric under the reflection. This symmetry forbids the cross point to be resolved as Fig.1(b). We can also assign the relevant topological invariant. By combining the magnetic mirror reflection with the particle-hole symmetry in the superconducting state, we can introduce chiral operator Γ which anticommutes with the Hamiltonian on the mirror plane. For example, the Hamiltonian in Eq. (1) anticommutes with $\Gamma = \tau_x$ at $k_y = 0$ and π. The chiral operator enables us to define the winding number [50]. For the present model, we find that the winding number is nonzero when k_z is on the vertical flat band at $k_y = 0$, while it changes the value at point nodes and disappears outside the Fermi surface. Thus, the vertical zero energy flat band at $\bar{k}_y = 0$ is topologically protected, although it connects nodes (or antinodes) with the same charge. Consequently, the cross point cannot be resolved in order to keep consistent topological flows.

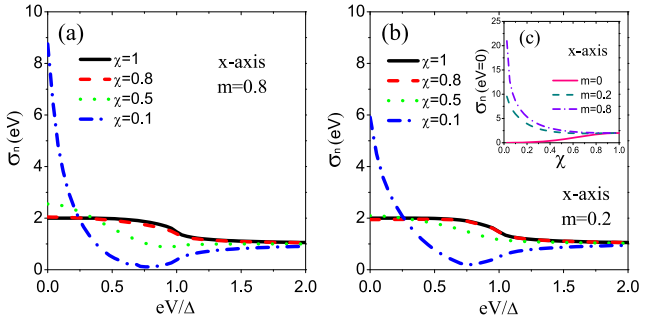


FIG. 4. (color online). Normalized tunneling conductance as a function of bias voltage (eV/Δ) for m equal to (a) 0.8 and (b) 0.2. (c) Relation between height of normalized ZBCP and χ. Other parameters are as the same as in Fig.2.

Experimental Signatures.– To explore the experimental signatures of the newly discovered SABSs, we consider a normal metal/superconductor (NS) junction in a doped WSM and calculate the normalized tunneling conductance $\sigma_{\rm n}(eV) = \sigma_{\rm S}(eV)/\sigma_{\rm N}(eV)$ using the tight binding model in Eq.(1) with an appropriate boundary condition [51, 52]. Here $\sigma_{\rm S}(eV)$ is the conductance of the NS junction, and $\sigma_{\rm N}(eV)$ is that in the normal state. We denote the transmissivity at the interface by χ, where $\chi = 0$ ($\chi = 1$) corresponds to the low transparent limit (full transmissivity)[52].

Figures 4(a) and (b) show the tunneling conductance $\sigma_{\rm n}$ in the x direction. The obtained $\sigma_{\rm n}$ shows zero-bias conductance peaks (ZBCPs), where the peak height is inversely proportional to χ, as shown in Fig.4(c). Such features are rather similar to those of d-wave supercondcutors with line nodes [45, 53–55], but not those of Sr_2RuO_4, which is a superconducting analog of the ^{3}He-A phase [56] or a ferromagnet/superconductor junction on the surface of a topological insulator [57]. Although the chiral p-wave state supports a vertical flat band, such a huge σ_n at $eV = 0$ cannot be obtained. In contrast, the crossing point of the flat bands in the superconducting WSMs forms a saddle point in the energy dispersion, producing a Van Hove singularity in the surface density of states. As a result, the ZBCP is very prominent.

Summary and Discussions.–So far we have reported that WSMs with surface Fermi arcs may support even more exotic crossed surface flat bands in the superconducting state. We found that the nontrivial topology of their normal state results in bulk point nodes in the s-wave pairing state, which enables us to design such nontrivial structure in condensed matter physics. We have also revealed that the crossed flat band structure is protected by magnetic mirror reflection symmetry. Conversely, the latter result implies that we can control the crossed flat bands by the perturbations which break the symmetry, e.g., the magnetic field along the y-axis.

Here we would like to compare our system with superfluid ^{3}He-A phase. Whereas superconducting WSMs support bulk point nodes similar to the A-phase bulk [26], we have found an important topological difference: The ^{3}He-A phase supports a node-antinode pair with opposite monopole charge in the Fermi surface, and thus, without topological twist, a surface flat band starts at the projection of a node on the surface BZ and ends at that of an antinode [58, 59], as shown in Fig.1(c). In contrast, the superconducting WSMs have nodes with the same charge, so the twisting of surface bands may occur.

In closing, we remark on the possible generalization of this work. Our topological arguments require three conditions. The first is a uniform pairing state. A nonuniform pairing state such as the FFLO state mixes the Chern numbers with different momenta, so it may destroy the topology of WSMs relevant to the crossed flat bands. The second is broken time-reversal symmetry in WSMs. For time-reversal-symmetric WSMs, the Chern numbers of electrons and of holes are canceled, so superconducting states cannot dominate the nontrivial topology of WSMs. The final condition is magnetic mirror reflection symmetry, which stabilizes the crossed flat bands. Once these three conditions are met, we may have crossed surface flat bands for any pairing state. Although an unconventional Cooper pair may create additional nodes on the Fermi surface, the total number of monopole charges should be nonzero, which allows the hosting of such complicated flat bands.

We thank A. Yamakage for useful discussion. This work was supported in part by Grants-in-Aid for Scientific Research from the Ministry of Education, Culture, Sports, Science and Technology of Japan ("Topological Quantum Phenomena" No. 22103005 and No. 25287085) and by the EU-Japan program "IRON SEA."

[1] S. Murakami, New J. Phys. **9**, 356 (2007).
[2] X. Wan, A. M. Turner, A. Vishwanath, and S. Y. Savrasov, Phys. Rev. B **83**, 205101 (2011).
[3] G. Xu, H. Weng, Z. Wang, X. Dai, and Z. Fang, Phys. Rev. Lett. **107**, 186806 (2011).
[4] A. A. Burkov and L. Balents, Phys. Rev. Lett. **107**, 127205 (2011).
[5] W. Witczak-Krempa and Y. B. Kim, Phys. Rev. B **85**, 045124 (2012).
[6] G. Chen and M. Hermele, Phys. Rev. B **86**, 235129 (2012).
[7] H.-J. Kim, K.-S. Kim, J.-F. Wang, V. A. Kulbachinskii, K. Ogawa, M. Sasaki, A. Ohnishi, M. Kitaura, Y.-Y. Wu, L. Li, I. Yamamoto, J. Azuma, M. Kamada, and V. Dobrosavljević, Phys. Rev. Lett. **110**, 136601 (2013).
[8] P. Hosur and X. Qi, Comptes Rendus Physique **14**, 857 (2013).
[9] T. Morimoto and A. Furusaki, preprint, Phys. Rev. B **89**, 235127 (2014).
[10] S. L. Adler, Phys. Rev. **177**, 2426 (1969).
[11] J. Bell and R. Jackiw, Nuovo Cimento A **60**, 47 (1969).
[12] H. Nielsen and M. Ninomiya, Physics Letters B **130**, 389 (1983).
[13] V. Aji, Phys. Rev. B, **85**, 241101 (2012)
[14] A. A. Zyuzin and A. A. Burkov, Phys. Rev. B **86**, 115133 (2012).
[15] C.-X. Liu, P. Ye, and X.-L. Qi, Phys. Rev. B **87**, 235306 (2013).
[16] M. N. Chernodub, A. Cortijo, A. G. Grushin, K. Landsteiner, and M. A. H. Vozmediano, Phys. Rev. B **89**, 081407 (2014).
[17] K. Landsteiner, Phys. Rev. B **89**, 075124 (2014).
[18] Z. Wang and S.-C. Zhang, Phys. Rev. B **87**, 161107 (2013).
[19] H. Ooguri and M. Oshikawa, Phys. Rev. Lett. **108**, 161803 (2012).
[20] Y. Chen, S. Wu, and A. A. Burkov, Phys. Rev. B **88**, 125105 (2013).
[21] C. Fang, M. J. Gilbert, X. Dai, and B. A. Bernevig, Phys. Rev. Lett. **108**, 266802 (2012).
[22] D. Kurebayashi and K. Nomura, J. Phys. Soc. Jpn. **83**, 063709 (2014).
[23] A. A. Burkov, M. D. Hook and L. Balents, Phys. Rev. B **84**, 235126 (2011).
[24] F. D. M. Haldane, preprint, arXiv:1401.0529 (2014).
[25] A. Damascelli, Z. Hussain, and Z.-X. Shen, Rev. Mod. Phys. **75**, 473 (2003).
[26] G. Y. Cho, J. H. Bardarson, Y.-M. Lu, and J. E. Moore, Phys. Rev. B **86**, 214514 (2012).
[27] V. Shivamoggi and M. J. Gilbert, Phys. Rev. B **88**, 134504 (2013).
[28] H. Wei, S.-P. Chao, and V. Aji, Phys. Rev. B **89**, 014506 (2014).
[29] H. Wei, S.-P. Chao, and V. Aji, Phys. Rev. B **89**, 235109 (2014).
[30] T. H. Hsieh and L. Fu, Phys. Rev. Lett. **108**, 107005 (2012).
[31] A. Yamakage, K. Yada, M. Sato, and Y. Tanaka, Phys. Rev. B **85**, 180509 (2012).
[32] S. Takami, K. Yada, A. Yamakage, M. Sato, and Y. Tanaka, J. Phys. Soc. Jpn. **83**, 064705 (2014).
[33] Junwei Liu, Timothy H. Hsieh, Peng Wei, Wenhui Duan, Jagadeesh Moodera and Liang Fu, Nature Materials **13**, 178 (2014).
[34] K.-Y. Yang, Y.-M. Lu, and Y. Ran, Phys. Rev. B **84**, 075129 (2011).
[35] M. Sato, Phys. Lett. B **575** 126 (2003).
[36] L. Fu and C. L. Kane, Phys. Rev. Lett. **100**, 096407 (2008).
[37] M. Sato, Y. Takahashi, and S. Fujimoto, Phys. Rev. Lett. **103**, 020401 (2009).
[38] J. Alicea, Phys. Rev. B **81**, 125318 (2010).
[39] J. D. Sau, R. M. Lutchyn, S. Tewari, and S. Das Sarma, Phys. Rev. Lett. **104**, 040502 (2010).
[40] R. M. Lutchyn, J. D. Sau, and S. Das Sarma, Phys. Rev. Lett. **105**, 077001 (2010).
[41] Y. Oreg, G. Refael, and F. von Oppen, Phys. Rev. Lett. **105**, 177002 (2010).
[42] L. J. Buchholtz and G. Zwicknagl, Phys. Rev. B **23**, 5788 (1981).
[43] J. Hara and K. Nagai, Prog. Theor. Phys. **76**, 1237 (1986).
[44] C. R. Hu, Phys. Rev. Lett. **72**, 1526 (1994).
[45] S. Kashiwaya and Y. Tanaka, Rep. Prog. Phys. **63**, 1641 (2000).
[46] A. P. Schnyder, S. Ryu, A. Furusaki, and A. W. W. Ludwig, Phys. Rev. B **78**, 195125 (2008).
[47] M. Sato, Y. Tanaka, K. Yada, and T. Yokoyama, Phys. Rev. B **83**, 224511 (2011).
[48] Y. Tanaka, M. Sato, and N. Nagaosa, J. Phys. Soc. Jpn. **81**, 011013 (2012).
[49] A. Umerski, Phys. Rev. B **55**, 5266 (1997).
[50] For more detailed topological arguments, see the Supplementary Materials.
[51] Q.-G. Zhu and H. Kroemer, Phys. Rev. B **27**, 3519 (1983).
[52] See the supplementary materials.
[53] Y. Tanaka and S. Kashiwaya, Phys. Rev. Lett. **74**, 3451 (1995).
[54] T. Löfwander, V. S. Shumeiko, and G. Wendin, Supercond. Sci. Technol. **14**, R53 (2001).
[55] C. L. M. Wong and K. T. Law, Phys. Rev. B **86**, 184516 (2013).
[56] M. Yamashiro, Y. Tanaka, and S. Kashiwaya, Phys. Rev. B **56**, 7847 (1997).
[57] Y. Tanaka, T. Yokoyama, and N. Nagaosa, Phys. Rev. Lett. **103**, 107002 (2009).
[58] G. E. Volovik, *The Universe in a Helium Droplet* (Oxford University Press, Oxford, UK, 2009).
[59] G. E. Volovik, JETP Lett. **93**, 66 (2011).

Supplementary Materials

S1. Magnetic mirror reflection symmetry

Here we discuss magnetic mirror reflection symmetry in WSMs. The magnetic mirror reflection symmetry is a combined symmetry of mirror reflection and time-reversal. As discussed below, many WSMs naturally have mirror reflection symmetry in a certain direction.

First, it should be noted that broken time-reversal is necessary to obtain a nonzero Chern number $C_1(k_z)$ in inversion symmetric WSMs. At the same time, we would like to point out that for the nonzero Chern number $C_1(k_z)$, reflection symmetries in directions normal to the z-axis must be broken. Because the flux $[\nabla_{\boldsymbol{k}} \times \mathcal{A}(\boldsymbol{k})]_z$ is odd under time-reversal and the reflection, each of these symmetries forces the integral $C_1(k_z) = \frac{1}{2\pi}\int d^2k [\nabla_{\boldsymbol{k}} \times \mathcal{A}(\boldsymbol{k})]_z$ to be zero.

Although each of them must be broken, their combined symmetry is consistent with inversion symmetric WSMs. Actually, we find that WSMs in pyrochlore iridates and $HgCr_2Se_4$ retain such magnetic mirror reflection symmetry. In both WSMs, the magnetic mirror reflection with respect to the (110) plane is preserved. This fact could be physically understood as a consequence that magnetic orders of these materials, which are necessary for nonzero $C_1(k_z)$, keep symmetry of the original materials as much as possible. We also find that a WSM in a topological insulator multilayer proposed in Ref.[S1] has a similar magnetic mirror reflection symmetry. Therefore, if Cooper pairs do not break the magnetic reflection symmetry, then the corresponding superconducting phase also retains the magnetic reflection symmetry.

Now we argue the magnetic mirror reflection symmetry in our model,

$$\begin{aligned}\mathcal{H}_{\mathbf{k}} = {} & t\sin k_x \sigma_y \tau_z - t \sin k_y \sigma_x \tau_0 + (t_z \cos k_z - M)\sigma_z \tau_z \\ & + m(2 - \cos k_x - \cos k_y)\sigma_z \tau_z - \mu \sigma_0 \tau_z - \Delta \sigma_y \tau_y. \end{aligned} \tag{S1}$$

The time-reversal operator is given by

$$T = -i\sigma_y \mathcal{K} \tau_0. \tag{S2}$$

with complex conjugation operator $\mathcal{K}$, and the mirror reflection operator is given by

$$M_{xz} = i\sigma_y \tau_0, \tag{S3}$$

and each of these symmetries is broken in our model,

$$T\mathcal{H}_{(k_x,k_y,k_z)}T^{-1} \neq \mathcal{H}_{(-k_x,-k_y,-k_z)}, \quad M_{xz}\mathcal{H}_{(k_x,-k_y,k_z)}M_{xz}^{-1} \neq \mathcal{H}_{(k_x,k_y,k_z)}. \tag{S4}$$

However, combining these two operators T and M_{xz}, we can define time-reversal like operator $\tilde{T} = M_{xz}T$, which satisfies

$$\tilde{T}\mathcal{H}_{(k_x,k_y,k_z)}\tilde{T}^{-1} = \mathcal{H}_{(-k_x,k_y,-k_z)}. \tag{S5}$$

This is the magnetic mirror reflection symmetry. Combining with the particle-hole symmetry of the BdG Hamiltonian,

$$C\mathcal{H}_{(-k_x,-k_y,-k_z)}C^{-1} = -\mathcal{H}_{(k_x,k_y,k_z)}, \tag{S6}$$

with

$$C = \sigma_0 \mathcal{K} \tau_x, \tag{S7}$$

we also obtain the *mirror chiral symmetry*

$$\Gamma\mathcal{H}_{(k_x,k_y,k_z)}\Gamma^{-1} = -\mathcal{H}_{(k_x,-k_y,k_z)}. \tag{S8}$$

with

$$\Gamma = C\tilde{T} \tag{S9}$$

This symmetry stabilizes the crossed surface flat bands as illustrated in Fig.1(b) in the main text: Equation (S8) implies that the flat bands with zero energy should be symmetric under $k_y \to -k_y$. Therefore, a problematic

reconnection process in Fig.1(c) in the main text never happens as far as the magnetic mirror reflection symmetry (and the resultant magnetic chiral symmetry) is present.

S2. Winding number

In this section, we show that the vertical flat band in Fig.2 in the main text has a non-trivial topological number defined by mirror chiral symmetry in Eq.(S8). At $k_y = 0, \pi$, the mirror chiral symmetry reduces to

$$\{\Gamma, \mathcal{H}_{(k_x,k_y,k_z)}|_{k_y=0,\pi}\} = 0, \tag{S10}$$

so we can define the following one-dimensional winding number for fixed k_z[S2],

$$W = -\frac{1}{4\pi i}\int_{-\pi}^{\pi} dk_x \mathrm{tr}\left[\Gamma \mathcal{H}_{\boldsymbol{k}}^{-1}\partial_{k_x}\mathcal{H}_{\boldsymbol{k}}\right]_{k_y=0,\pi} \tag{S11}$$

Following the discussion in Ref.[S3], we can transform $\mathcal{H}_{\mathbf{k}}$ into anti-diagonalized form by unitary matrix U:

$$U\mathcal{H}_{\mathbf{k}}U^{\dagger} = \begin{pmatrix} 0 & q\left(\mathbf{k}\right) \\ q^{\dagger}\left(\mathbf{k}\right) & 0 \end{pmatrix}, \tag{S12}$$

with

$$q\left(\mathbf{k}\right) = \begin{pmatrix} -\mu + D\left(\mathbf{k}\right) & -\Delta - it\sin k_x \\ \Delta + it\sin k_x & -\mu - D\left(\mathbf{k}\right) \end{pmatrix} \tag{S13}$$

and with $D\left(\mathbf{k}\right) = t_z\cos k_z - M + m(2 - \cos k_y - \cos k_x)$. Using a parameter $\theta = \arg(\det q(\mathbf{k}))$, the winding number W at $k_y = 0$ or π can be evaluated as defined as [S4]:

$$W = \frac{1}{2\pi}\int_{-\pi}^{\pi}\frac{\partial\theta}{\partial k_x}dk_x. \tag{S14}$$

After a straightforward calculation, we obtain for $\Delta > 0$

$$W_{k_y=0}\left(k_z\right) = \frac{1}{2}[\mathrm{sgn}\left(\omega_1\right) - \mathrm{sgn}\left(\omega_2\right)], \tag{S15}$$

$$W_{k_y=\pi}\left(k_z\right) = \frac{1}{2}[\mathrm{sgn}\left(\omega_2\right) - \mathrm{sgn}\left(\omega_3\right)], \tag{S16}$$

where $\omega_1 = \Delta^2 + \mu^2 - (t_z\cos k_z - M)^2$, $\omega_2 = \Delta^2 + \mu^2 - (t_z\cos k_z - M + 2m)^2$ and $\omega_3 = \Delta^2 + \mu^2 - (t_z\cos k_z - M + 4m)^2$. In Fig.3(b)in the main text, we find that the winding number is nonzero when k_z is on the vertical flat band at $k_y = 0$. The winding number disappears at point nodes and it remains zero outside the Fermi surface. A more complicated case is also illustrated in Fig.3(d) in the main text.

Similar type of flat bands of SABS as Majorana fermions is discussed in non-centrosymmetric superconductors [S5–S9] and spin-orbit coupled systems[S2, S10–S14].

S3. Tunneling conductance

To calculate the tunneling conductance of NS (normal metal / superconductor) junction based on the tight-binding model in Eqs. (1) and (2) in the main text, we express the Hamiltonian H in a lattice space, which is given by

$$\begin{aligned} H = &\sum\nolimits_{ijn} it(-\bar{c}^{\dagger}_{i,j,n}\sigma_y\bar{c}_{i+1,j,n} + \bar{c}^{\dagger}_{i,j,n}\sigma_y\bar{c}_{i-1,j,n} + \bar{c}^{\dagger}_{i,j,n}\sigma_x\bar{c}_{i,j+1,n} - \bar{c}^{\dagger}_{i,j,n}\sigma_x\bar{c}_{i,j-1,n})/2 \\ &+t_z(\bar{c}^{\dagger}_{i,j,n}\sigma_z\bar{c}_{i,j,n+1} + \bar{c}^{\dagger}_{i,j,n}\sigma_z\bar{c}_{i,j,n-1})/2 + (2m - t_z\cos Q)\,\bar{c}^{\dagger}_{i,j,n}\sigma_z\bar{c}_{i,j,n} \\ &-m(\bar{c}^{\dagger}_{i,j,n}\sigma_z\bar{c}_{i+1,j,n} + \bar{c}^{\dagger}_{i,j,n}\sigma_z\bar{c}_{i-1,j,n} + \bar{c}^{\dagger}_{i,j,n}\sigma_z\bar{c}_{i,j+1,n} + \bar{c}^{\dagger}_{i,j,n}\sigma_z\bar{c}_{i,j-1,n})/2 \\ &-\mu\bar{c}^{\dagger}_{i,j,n}\bar{c}_{i,j,n} + \Delta c^{\dagger}_{i,j,n\uparrow}c^{\dagger}_{i,j,n\downarrow} + \Delta c_{i,j,n\downarrow}c_{i,j,n\uparrow}, \end{aligned} \tag{S17}$$

with $\bar{c}_{ijn} = (c_{ijn\uparrow}, c_{ijn\downarrow})^T$. Here, i, j, and n denote the site indexes in x, y and z directions, respectively. We assume the spatial dependence of the pair potential as $\Delta = \Delta_0\,(zero)$ with $i \geq 1\ (< 1)$ for junctions along x-axis and $\Delta = \Delta_0\,(zero)$ with $n \geq 1\ (< 1)$ for those along z-axis.

By applying the Bogoliubov transformation in the above lattice Hamiltonian

$$c_{ijn\sigma} = \sum\nolimits_{\nu} u^{\nu}_{ijn\sigma}\hat{\gamma}_{\nu} + v^{\nu *}_{ijn\sigma}\hat{\gamma}^{\dagger}_{\nu}, \tag{S18}$$

we can obtain the lattice version of the BdG equations

$$\begin{cases} \varepsilon_\nu u^\nu_{ijn\uparrow} = (-tu^\nu_{i+1,jn\downarrow} + tu^\nu_{i-1,jn\downarrow} + itu^\nu_{i,j+1,n\downarrow} - itu^\nu_{i,j-1,n\downarrow} + t_z u^\nu_{ij,n+1\uparrow} + t_z u^\nu_{ij,n-1\uparrow})/2 + \\ \quad (2m - t_z\cos Q - \mu)\, u^\nu_{ijn\uparrow} - m(u^\nu_{i+1,jn\uparrow} + u^\nu_{i-1,jn\uparrow} + u^\nu_{i,j+1,n\uparrow} + u^\nu_{i,j-1,n\uparrow})/2 + \Delta v^\nu_{ijn\downarrow}, \\ \varepsilon_\nu u^\nu_{ijn\downarrow} = (tu^\nu_{i+1,jn\uparrow} - tu^\nu_{i-1,jn\uparrow} + itu^\nu_{i,j+1,n\uparrow} - itu^\nu_{i,j-1,n\uparrow} - t_z u^\nu_{ij,n+1\downarrow} - t_z u^\nu_{ij,n-1\downarrow})/2 + \\ \quad (-2m + t_z\cos Q - \mu)\, u^\nu_{ijn\downarrow} + m(u^\nu_{i+1,jn\downarrow} + u^\nu_{i-1,jn\downarrow} + u^\nu_{i,j+1,n\downarrow} + u^\nu_{i,j-1,n\downarrow})/2 - \Delta v^\nu_{ijn\uparrow}, \\ \varepsilon_\nu v^\nu_{ijn\uparrow} = (tv^\nu_{i+1,jn\downarrow} - tv^\nu_{i-1,jn\downarrow} + itv^\nu_{i,j+1,n\downarrow} - itv^\nu_{i,j-1,n\downarrow} - t_z v^\nu_{ij,n+1\uparrow} - t_z v^\nu_{ij,n-1\uparrow})/2 + \\ \quad (-2m + t_z\cos Q + \mu)\, v^\nu_{ijn\uparrow} + m(v^\nu_{i+1,jn\uparrow} + v^\nu_{i-1,jn\uparrow} + v^\nu_{i,j+1,n\uparrow} + v^\nu_{i,j-1,n\uparrow})/2 - \Delta u^\nu_{ijn\downarrow}, \\ \varepsilon_\nu v^\nu_{ijn\downarrow} = (-tv^\nu_{i+1,jn\uparrow} + tv^\nu_{i-1,jn\uparrow} + itv^\nu_{i,j+1,n\uparrow} - itv^\nu_{i,j-1,n\uparrow} + t_z v^\nu_{ij,n+1\downarrow} + t_z v^\nu_{ij,n-1\downarrow})/2 + \\ \quad (2m - t_z\cos Q + \mu)\, v^\nu_{ijn\downarrow} - m(v^\nu_{i+1,jn\downarrow} + v^\nu_{i-1,jn\downarrow} + v^\nu_{i,j+1,n\downarrow} + v^\nu_{i,j-1,n\downarrow})/2 + \Delta u^\nu_{ijn\uparrow}. \end{cases} \tag{S19}$$

Here, wave functions of the NS junction can be written as

$$\Psi^N_\alpha(\mathbf{r}) = \sum\nolimits_\beta \left[\xi^e_\alpha(\mathbf{r}) + r^e_{\alpha\beta}\xi^e_\beta(\mathbf{r}) + r^h_{\alpha\beta}\xi^h_\beta(\mathbf{r})\right], \tag{S20}$$

$$\Psi^S_\alpha(\mathbf{r}) = \sum\nolimits_\delta \left[t^e_{\alpha\delta}\eta^e_\delta(\mathbf{r}) + t^h_{\alpha\delta}\eta^h_\delta(\mathbf{r})\right], \tag{S21}$$

where α, β and δ denote corresponding Weyl cones. The spinors $\xi^{e(h)}(\mathbf{r})$ and $\eta^{e(h)}(\mathbf{r})$ can be solved by Eq.(S19):

$$\xi^e(\mathbf{r}) = \frac{1}{\sqrt{N_e}} \begin{pmatrix} t\left(i\sin k^e_x + \sin k^e_y\right) \\ \mathcal{M}\left(k^e_x, k^e_y, k^e_z\right) - \mu - E \\ 0 \\ 0 \end{pmatrix} e^{i(k^e_x x + k^e_y y + k^e_z z)}, \tag{S22}$$

$$\xi^h(\mathbf{r}) = \frac{1}{\sqrt{N_h}} \begin{pmatrix} 0 \\ 0 \\ -t\left(i\sin k^h_x - \sin k^h_y\right) \\ -\mathcal{M}\left(k^h_x, k^h_y, k^h_z\right) + \mu - E \end{pmatrix} e^{i(k^h_x x + k^h_y y + k^h_z z)}, \tag{S23}$$

with

$$\mathcal{M}(k_x, k_y, k_z) = t_z(\cos k_z - \cos Q) + m(2 - \cos k_x - \cos k_y), \tag{S24}$$

and

$$\eta(\mathbf{r}) = \frac{1}{\sqrt{N_S}} \begin{pmatrix} \left[\mathcal{G}(p_x, p_y, p_z) - (\mu - E)^2 + \Delta_0^2\right](t\sin p_x - it\sin p_y) \\ i\left[\mathcal{G}(p_x, p_y, p_z) - (\mu - E)^2\right][\mu + E - \mathcal{M}(p_x, p_y, p_z)] + [-\mu + E + \mathcal{M}(p_x, p_y, p_z)]\,\Delta_0^2 \\ i\left\{-\mu^2 + [E - \mathcal{M}(p_x, p_y, p_z)]^2 - t^2\left(\sin^2 p_x + \sin^2 p_y\right) - \Delta^2\right\}\Delta_0 \\ 2(\mu - \mathcal{M}(p_x, p_y, p_z))(t\sin p_x - it\sin p_y)\,\Delta_0 \end{pmatrix} e^{i(p_x x + p_y y + p_z z)}, \tag{S25}$$

with

$$\mathcal{G}(p_x, p_y, p_z) = \mathcal{M}^2(p_x, p_y, p_z) + t^2\left(\sin^2 p_x + \sin^2 p_y\right). \tag{S26}$$

Here, N_e, N_h, and N_S are normalization constants. $k^{e(h)}_x$, $k^{e(h)}_y$ and $k^{e(h)}_z$ satisfy the dispersion relation

$$E^e = \sqrt{\mathcal{G}\left(k^e_x, k^e_y, k^e_z\right)} - \mu, \tag{S27}$$

$$E^h = -\sqrt{\mathcal{G}\left(k^h_x, k^h_y, k^h_z\right)} + \mu, \tag{S28}$$

and p_x, p_y and p_z satisfy

$$E^S = \sqrt{\left(\mu - \sqrt{\mathcal{G}(p_x, p_y, p_z) + \left(\mathcal{M}(p_x, p_y, p_z)\,\Delta_0/\mu\right)^2}\right)^2 + \Delta_0^2\left(1 - \mathcal{M}^2(p_x, p_y, p_z)/\mu^2\right)}. \tag{S29}$$

Using the boundary condition[S15]:

$$\hat{t}\Psi_{\alpha}^{N}\left(i=1\right)=\chi\hat{t}\Psi_{\alpha}^{S}\left(i=1\right), \tag{S30}$$
$$\chi\hat{t}'\Psi_{\alpha}^{N}\left(i=0\right)=\hat{t}'\Psi_{\alpha}^{S}\left(i=0\right), \tag{S31}$$

for the junction along x-axis and

$$\hat{t}_{z}\Psi_{\alpha}^{N}\left(n=1\right)=\chi\hat{t}_{z}\Psi_{\alpha}^{S}\left(n=1\right), \tag{S32}$$
$$\chi\hat{t}_{z}'\Psi_{\alpha}^{N}\left(n=0\right)=\hat{t}_{z}'\Psi_{\alpha}^{S}\left(n=0\right), \tag{S33}$$

for the junction along z-axis, one can obtain the coefficients $r_{\alpha\beta}^{e(h)}$ and $t_{\alpha\delta}^{e(h)}$. Here, $\hat{t}$ and $\hat{t}_z$ represent the effective hopping term in BdG equations given by

$$\hat{t}=\left(-it\sigma_{y}\tau_{z}-m\sigma_{z}\tau_{z}\right)/2, \tag{S34}$$
$$\hat{t}'=\left(it\sigma_{y}\tau_{z}-m\sigma_{z}\tau_{z}\right)/2, \tag{S35}$$
$$\hat{t}_{z}=\hat{t}_{z}'=t_{z}\sigma_{z}\tau_{z}/2. \tag{S36}$$

We define χ to describe the transmissivity of NS junction. $\chi=0$ ($\chi=1$) corresponds to the edge (perfect transmitting junction). Finally, we obtain the charge current:

$$I\left(V\right)=\eta_{1}\int dE\left[f\left(E-eV\right)-f\left(E\right)\right]\sigma_{S}\left(E\right), \tag{S37}$$

where

$$\sigma_{S}\left(E\right)=\eta_{2}\sum\nolimits_{\alpha,\mathbf{k}_{\parallel}}\sigma_{S}^{\alpha}\left(E,\mathbf{k}_{\parallel}\right), \tag{S38}$$

$$\sigma_{S}^{\alpha}\left(E,\mathbf{k}_{\parallel}\right)=\sum\nolimits_{\beta}\mathrm{Re}[1-\frac{v_{\beta}^{(e)}\left(E\right)}{v_{\alpha}^{(e)}\left(E\right)}\left|r_{\alpha\beta}^{e}\right|^{2}+\frac{v_{\beta}^{(h)}\left(E\right)}{v_{\alpha}^{(e)}\left(E\right)}\left|r_{\alpha\beta}^{h}\right|^{2}]. \tag{S39}$$

The summation runs over all the indices of Weyl cones α and $\mathbf{k}_{\parallel}$. The quantity $\mathbf{k}_{\parallel}$ denotes (k_x, k_y) and (k_y, k_z) in the junction along x-axis and that along z-axis, respectively.

$v_{\beta}^{(e)}\left(E\right)$ are the group velocities which can be derived from dispersion relation of the bulk energy spectrum $\left(1/\hbar\right)\partial E/\partial k_{x}$. $\eta_{1(2)}$ is the constant determined by the geometry of the microconstruction. We calculate normalized conductance

$$\sigma_{n}\left(eV\right)=\sigma_{S}\left(eV\right)/\sigma_{N}\left(eV\right), \tag{S40}$$

where $\sigma_{N}\left(eV\right)$ is the conductance in the normal state. It is noted that $\eta_{1(2)}$ does not appear in the expression of the normalized conductance $\sigma_n(eV)$.

In the main text, we have shown that the zero biased conductance peak (ZBCP) emerges when the NS junction is along the x-direction. But as shown in Fig.S1 (a), the present ZBCP depends on m and it vanishes for $m=0$. This is consistent with the discussion based on the winding number in main text since the projected Fermi surfaces are overlapped and resulting surface Andreev bound states are absent for $m=0$. In the junction along z-axis, the resulting σ_n is insensitive to m. Since there is no surface Andreev bound states along this direction, ZBCP does not appear in the limit of low transmissivity $\chi\to 0$. The line shapes of σ_n are the essentially the same as those of the bulk density of states as shown in Fig.S1 (b).

[S1] A. A. Burkov and L. Balents, Phys. Rev. Lett. **107**, 127205 (2011).
[S2] M. Sato and S. Fujimoto, Phys. Rev. B **79**, 094504 (2009).
[S3] A. Ii, K. Yada, M. Sato, and Y. Tanaka, Phys. Rev. B **83**, 224524 (2011).
[S4] M. Sato, Y. Tanaka, K. Yada, and T. Yokoyama, Phys. Rev. B **83**, 224511 (2011).
[S5] P. Goswami and S. Tewari, Phys. Rev. B **88**, 245107 (2013).
[S6] J. D. Sau and S. Tewari, Phys. Rev. B **86**, 104509 (2012).
[S7] R. Queiroz and A. P. Schnyder, Phys. Rev. B **89**, 054501 (2014).

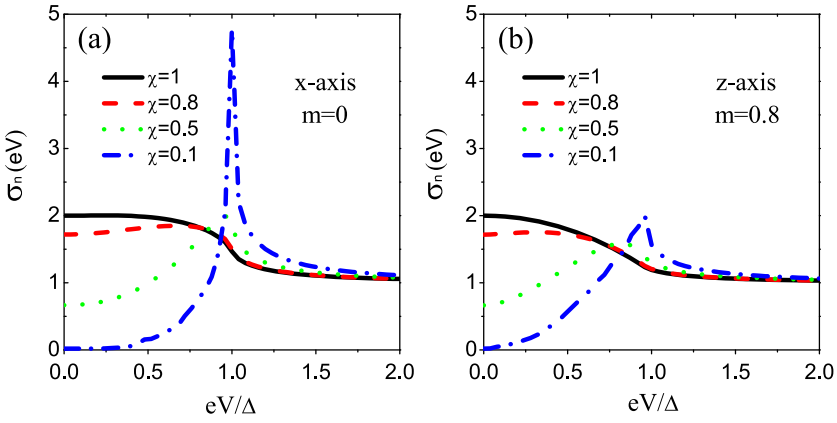


FIG. S1. (Color online) (a) Normalized tunneling conductance as a function of bias voltage (eV/Δ) for junctions along (a) x-axis with $m = 0$ and (b) z-axis with $m = 0.8$. Other parameters are as the same as in Fig.2 in the main text.

[S8] K. Yada, M. Sato, Y. Tanaka, and T. Yokoyama, Phys. Rev. B. **83**, 064505 (2011).
[S9] Y. Tanaka, Y. Mizuno, T. Yokoyama, K. Yada, and M. Sato, Phys. Rev. Lett. **105**, 097002 (2010).
[S10] M. Sato, Y. Takahashi, and S. Fujimoto, Phys. Rev. Lett. **103**, 020401 (2009).
[S11] J. Alicea, Phys. Rev. B **81**, 125318 (2010).
[S12] J. D. Sau, R. M. Lutchyn, S. Tewari, and S. Das Sarma, Phys. Rev. Lett. **104**, 040502 (2010).
[S13] Y. Oreg, G. Refael, and F. von Oppen, Phys. Rev. Lett. **105**, 177002 (2010).
[S14] R. M. Lutchyn, J. D. Sau, and S. Das Sarma, Phys. Rev. Lett. **105**, 077001 (2010).
[S15] Q.-G. Zhu and H. Kroemer, Phys. Rev. B **27**, 3519 (1983).